Enhancing bathymetric LiDAR by applying fractal dimensions to signal processing

Jan Rhomberg-Kauert[1], Lucas Dammert[1] and Gottfried Mandlburger[1]

[1]Department of Geodesy and Geoinformation, TU Wien; 1040 Vienna, Austria - jan.rhomberg-kauert@geo.tuwien.ac.at, lucas.dammert@geo.tuwien.ac.at, gottfried.mandlburger@geo.tuwien.ac.at

Keywords: laser scanning, laser bathymetry, full-waveform, fractal dimension, aquatic vegetation

Abstract

Fractal dimension is a statistical index of complexity to characterize geometries. It is commonly used in signal processing in different fields of research. There, observations of dynamic systems can be translated into numerical values allowing us to classify signals into groups of similar characteristics. In full-waveform LiDAR this methodology can be applied to the reflected echo pulse, thus enabling an analysis based on the overall waveform characteristics. Consequently, the fractal dimension of the full-waveform can be leveraged to differentiate between echo pulses with a high number of returns and single- or low-return echo pulses. This introduces an independent measure, which is calculated prior to the signal processing step. The advantage of this initial classification is that the echo pulse extraction could be further improved without need for human supervision, as the correlation between the number of echo pulses and the fractal dimension hints towards a measure of estimating the number of echo pulses within a recorded full-waveform. To conclude, we expand the concept of the fractal dimension to LiDAR waveforms and use the extracted correlation between the number of echo pulses and the fractal dimension to gain new insights for estimating the total number of echo pulses. This improvement is demonstrated through comparisons with manually annotated data, advancing the state-of-the-art in full-waveform analysis and introducing additional parameters.

1. Introduction

Full-waveform LiDAR has become an increasingly available commodity in the field of geospatial analysis (Mallet and Bretar, 2009; Mandlburger, 2022; Pfeifer and Briese, 2007). Through the detailed recording of the temporal record of the reflected echo pulse, the pulse-target interaction can be extracted as a sampled curve over time (RIEGL, Laser Measurement Systems GmbH, 2012). From this step onward, the standard workflow looks to extract the number of targets within the waveform. By determining the temporal position of the targets, their positions in the sensor frame of the laser scanner can be calculated. Furthermore, standard attributes such as amplitude and reflectance are extracted to provide further insight into the target properties (RIEGL, Laser Measurement Systems GmbH, 2012; Wagner et al., 2006). This well-studied field focuses on the deconvolution of the different echo pulses within the recorded waveform, rather than the waveform as a whole (Mandlburger et al., 2023b; Pfennigbauer et al., 2020). Therefore, initial echo pulse detection can potentially be further improved through research of the relation of the global waveform shape and the number of returns within (Schwarz et al., 2017; Ullrich and Pfennigbauer, 2011).

This is where the concept of the fractal dimension comes into play, as the fractal dimension captures the entire structure of the waveform and converts it into numerical values (Raghavendra and Narayana Dutt, 2009). This concept is well established in other fields of research where, e.g., the fractal dimension can be used to correlate periodic patterns with real-valued numbers (Esteller et al., 2001; Hoyer et al., 2020; Raghavendra and Narayana Dutt, 2009). For mathematical objects, the fractal dimension is a continuous extension of the Euclidean space. In the classical notation of dimensions, the perceived space has a natural dimension (three or four, including time). In contrast, the fractal dimension is expressed as a real number (Moriguchi, 2023). For example, the dimension of the Sierpinski triangle (Figure 1 A) is $\log_2 3$ and in the field of differential equations, the fractal dimension of the Lorenz attractor (Figure 1 B) can be approximated as 2.06 (Falconer, 2014; Lorenz, 1963; McGuinness, 1983). In mathematics, this definition is used to differentiate between degrees of complication for a geometric curve. In general, the tools of self-similarity can be used to investigate random phenomena in geostatistics, economics, and physics (Mandelbrot, 1967). There are many variants of the fractal dimension, and various algorithms have been proposed to compute them (Esteller et al., 2001; Raghavendra and Narayana Dutt, 2009; Yang et al., 2015). The two most common fractal dimensions mentioned in the literature are the Hausdorff dimension and the box counting dimension (also referred to as the Minkowski-Bouligand dimension) (Farmer et al., 1983; Mainieri, 1993; Moriguchi, 2023). Although both are similar, in the application-related fields the box-counting dimension has become the main tool for the analysis of dynamic signals, as there the effective estimation within the Euclidean space has proven advantageous (Ai et al., 2014; Fernández-Martínez and Sánchez-Granero, 2014). This expands the fractal dimension from mathematical objects to various applications such as images or signals, in which the box-counting method approximates the fractal dimension through linear regression in a log-log plot of the mesh size and the number of boxes that include part of the objects (Moriguchi, 2023; Yang et al., 2015). The extrac-

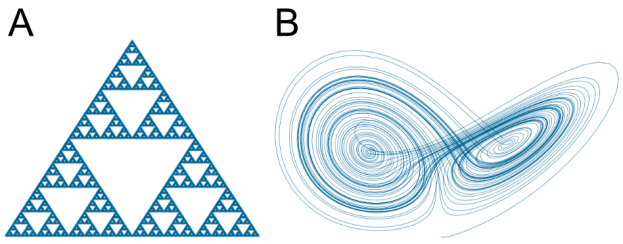

Figure 1. (A) The Sierpinski triangle (Sierpinski, 1915; Wahab, 2024) and (B) the Lorenz attractor (Hunter, 2007; Lorenz, 1963)

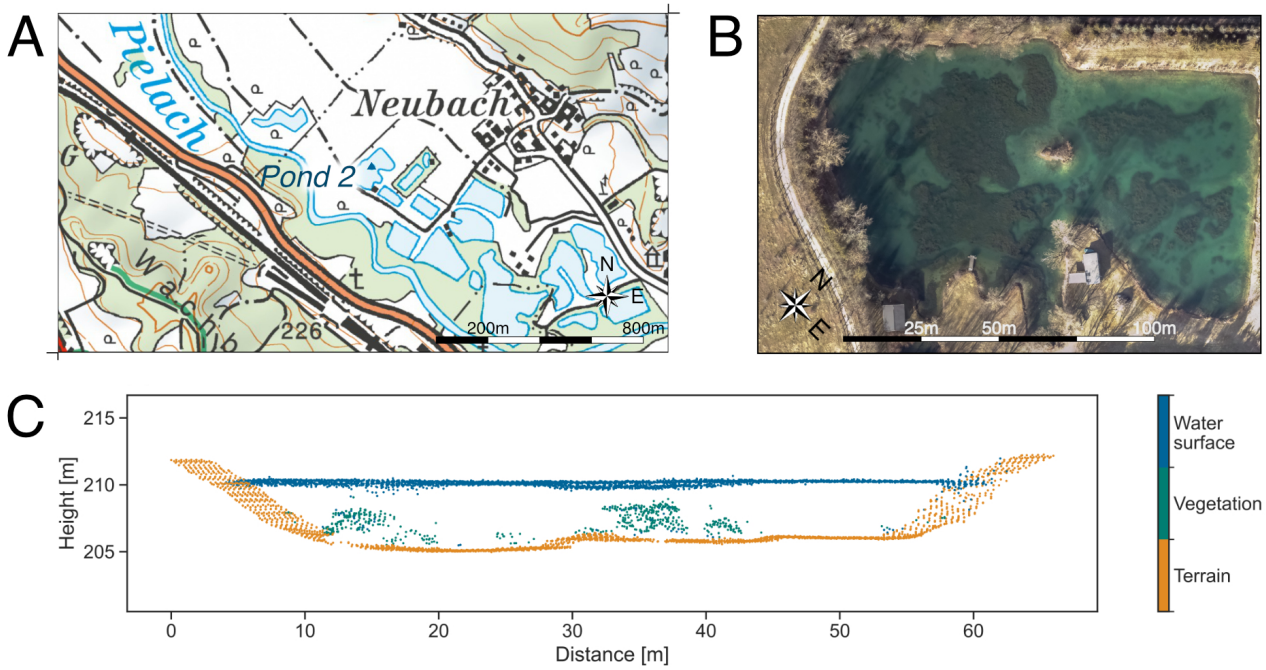

Figure 2. (A) Overview of the study area in Loosdorf (48.2010 N, 15.4004 E; WGS 84) Lower Austria (BEV, 2024). (B) Pond surveyed in February 2022 (48.2166 N, 15.3744 E) and (C) a cross-section of the pond with manually annotated classification labels.

ted numerical value can then be used for the classification of the signal and thus to improve the understanding of the structure of the underlying mechanics.

This methodology can also be applied to LiDAR, where the recorded waveform (a set of 2D points; amplitude × time) or the point cloud (a set of 3D points; x-y-z coordinates) can be used as input data to calculate the fractal dimension of the survey target. For terrestrial LiDAR, characterizations based on waveform structure have been proposed in the past (Heinzel and Koch, 2011; Mallet et al., 2008), where the shape and characteristics of the recorded signal are used to classify points into different categories. Examples are the different elements of urban environments or the differentiation of tree species. Additionally, for the classical structural analysis of point clouds, the fractal dimension has been applied to classify the point distributions of voxels, to estimate tree parameters (Moriguchi, 2023). In the case of bathymetric LiDAR, the focus is primarily on submerged targets. There, recent advances have improved the detection and classification of aquatic vegetation (Mandlburger et al., 2023b; Wagner et al., 2024). For such submerged targets, the return extraction from the waveform presents unique challenges, as the air-water medium change directly influences the overall waveform shape. Furthermore, signal absorption within the water column leads to weaker returns (Schwarz et al., 2017). This has led to a variety of methods that have been specifically developed to extract signals from full-waveform bathymetric LiDAR (Li et al., 2024; Schwarz et al., 2017, 2019). Here, the possibility to analyze the waveform as a whole and extract information about the number of echo pulses a priori remains. This information could potentially be applied to fine-tune extraction algorithms by setting limits or optimizing parameters in the classical peak detection through a threshold set by the fractal dimension.

Therefore, we introduce the concept of fractal dimensions for full-waveform LiDAR and show a correlation between the number of echo pulses and the fractal dimension. This generates a measure independent of other LiDAR attributes, which could improve waveform classification. Furthermore, the insights gained on the fractal dimension can be compared to human peak detection, and thus introduce a measure related to manual annotation. For this, the paper first introduces a suitable bathymetric LiDAR dataset, containing different waveforms of varying shapes (Section 2.1). Secondly, the fractal dimension is formally introduced and the specific application to LiDAR data is thoroughly explained (Section 2.3). Building on the methodology and data set introduced, the results display a correlation between the number of echo pulses and the fractal dimension and further explore the relation to the annotation of human peak (Section 3). Lastly, these results are discussed in light of current best practices in the full-waveform analysis (Section 4) and a summary of the findings is given (Section 5).

2. Materials and method

To investigate the concept of fractal dimensions for full-waveform LiDAR, this section first introduces a bathymetric LiDAR dataset acquired in 2022 containing a vegetated pond with a variety of different waveforms. After this initial introduction of the data, the formal definitions of the fractal dimensions are explained and the methodology for processing the waveform data is outlined, building the basis for the results reported in Section 3.

2.1 Dataset

The data set used in this study is located in Loosdorf (48.2010 N, 15.4004 E; WGS 84) in the region of Lower Austria (Mandlburger et al., 2023a). The region of interest is defined by the Pielach River and multiple freshwater ponds. In the surveyed area, a subset of these ponds contain visible vegetation. We choose Pond 2 for the analysis, which allows in-depth comparison of full-waveform data reflected by aquatic vegetation (Fig. 2). The data was acquired with the *RIEGL* VQ-840-G, a topo-bathymetric LiDAR system (Table 1). The measuring

platform was mounted on a helicopter and flown at an average altitude of 187 m on February, 9th, 2022. The system uses a wavelength of 532 nm and medium-sized footprints with an average footprint diameter of 0.93 m (RIEGL, Laser Measurement Systems GmbH, 2012; RIEGL, 2023).

System	Wavelength	Flight altitude	Beam divergence
LiDAR	532 nm	187 m ± 20 m	5 mrad

Table 1. Characteristics and parameters of the LiDAR system used in the survey.

The recorded waveforms were processed to generate a 3D point cloud for further structural analysis and to link the geometric features to the corresponding waveforms recorded by the LiDAR system. Through the combination of both the point cloud and the waveform recordings, a comprehensive dataset is obtained, providing the basis for the introduction of the fractal dimension analysis.

2.2 Manual peak annotation

The vegetation visible in the orthophoto of Figure 2 B causes multiple returns at varying depths within the pond. Therefore, the recorded waveforms include (i) single echo pulses on the surveyed terrain around the pond, (ii) two peak returns, where only the water surface and bottom are scanned, and (iii) multireturn echo pulses, where vegetation or other submerged targets are interacting with the signal in addition to the water surface and bottom. First, a subsample of the waveform data is selected by picking four different rounded fractal dimensions and extracting 25 waveforms for each category. In those selected waveforms, the number of returns ranges from single echos up to seven peaks detected by the SVB (Surface-Volume-Bottom) algorithm (Schwarz et al., 2019). To obtain a second independent count of the number of echo pulses for each waveform, two experts manually annotated a subset of the data. There, a representative subset of 100 waveforms was chosen from the data. In this subset, the number of echo pulses ranges from single returns up to eight peaks detected during point cloud extraction. Each annotation was done independently, thus allowing for a qualitative evaluation of the fractal dimension in the light of both state-of-the-art waveform fitting and supervised evaluation.

2.3 Fractal dimension

To calculate the box-counting dimension $\dim_{\text{box}}(S)$ of a non-empty bounded subset $S \subset \mathbb{R}^n$, we can draw a square cover on top of the set S and count the number of boxes $N(l)$ that overlap the set of length l for each square (Ai et al., 2014; Falconer, 2014). By decreasing the length l of the squares, the value $N(l)$ changes and, if the set S exhibits a fractal pattern, the Equation 1 for l and $N(l)$ holds true (Ai et al., 2014; Falconer, 2014).

$$N(l) \sim l^{-\dim_{\text{box}}(S)} \tag{1}$$

This relation can be leveraged, as visually the log transformed plot of both quantities forms a regression line with the slope of $-\dim_{\text{box}}(S)$ (Ai et al., 2014; Falconer, 2014). Therefore, the box-counting dimension can be estimated by the gradient of the graph of $\log(N(l))$ against $\log(l)$ given by

$$\dim_{\text{box}}(S) = -\lim_{l \to 0} \frac{\log(N(l))}{\log(l)} \tag{2}$$

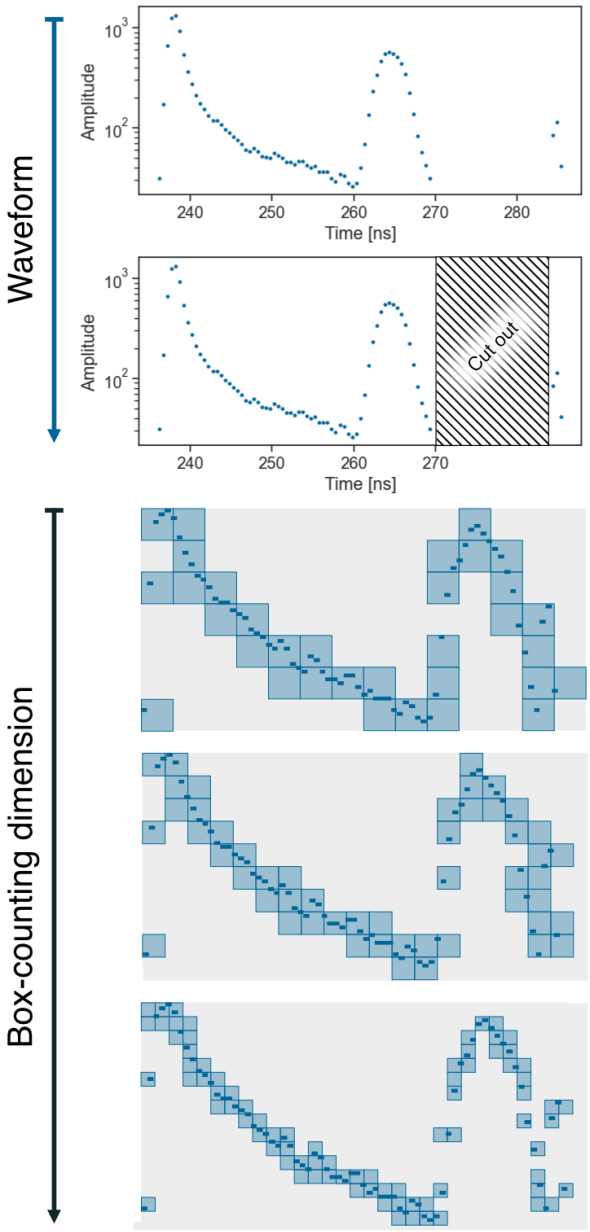

Figure 3. Workflow illustration for the fractal dimension calculation using the box-counting dimension. The first panel displays a scatter-plot of all recorded samples. Based on this input, the empty space within the signal (striped area) gets removed to improve computation time. The three following panels display the transformed waveform (from the waveform to a pixel image) and an illustration of the box-counting process.

In general terms, the relationship between intersecting sets of boxes and the length of the boxes can be seen as how irregular (spread out) the set is in relation to how fast the irregularities of the set S develop as l approaches 0 (Ai et al., 2014). The initial waveform, as recorded by the LiDAR system, consists of an intensity measurement and the time at which the sample was recorded (Figure 3). The waveform is recorded in a sparse format of 2D coordinates (time/intensity). Therefore, to use the tools provided by the box-counting dimension, the recorded points must be transformed into an image containing the recorded signal. This is done by transforming the signal into a matrix of dimension’s maximum intensity × length of the re-

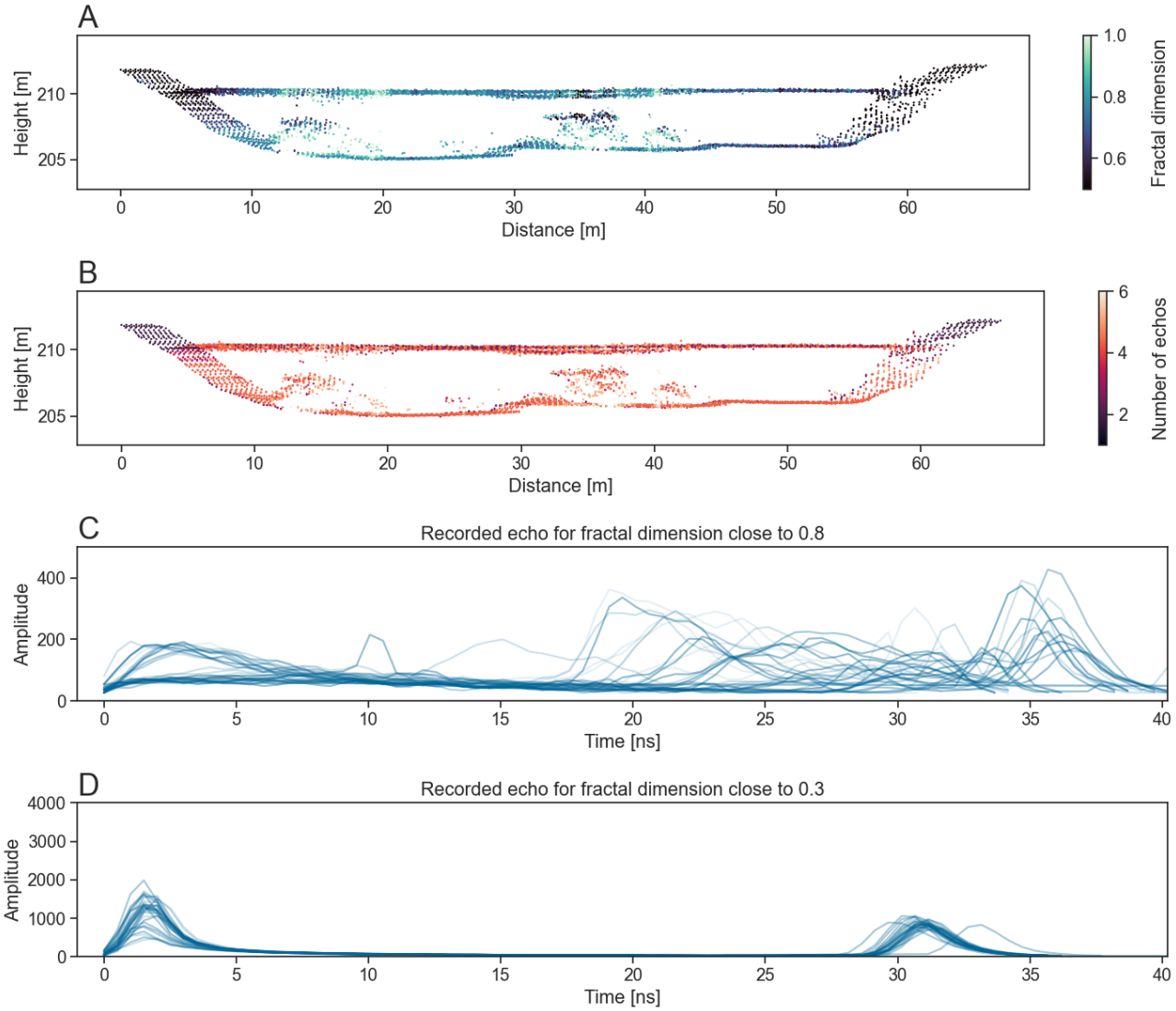

Figure 4. (A-B) Scatter plot of the cross-section from Figure 2 C, colored by the fractal dimension of the waveforms for each point and the number of echo pulses recorded. (C) Multi-plot of different waveforms with a rounded fractal dimension of 0.8, adjusted to have the same initial starting time. (D) Corresponding panel to C, with a rounded fractal dimension of 0.3.

cording. Each entry for which a signal is recorded is set to one, the rest is kept at zero. Furthermore, to reduce the size of the matrix and save computation time, all rows and columns with all zero entries are dropped, leaving only a minimal version of the signal as an image (Figure 3).

The resulting image can be used as input to the box-counting algorithm, and the fractal dimension of the visible signal can be estimated. Simplified, the method encompasses the waveform, displayed in the created image, in boxes of length l (Figure 3). This is done for continuously decreasing box sizes, and the number of boxes needed in relation to the overall image is tracked for each step l. The fractal dimension can then be approximated by fitting a regression line to all steps (Equation 2), where the negative slope of the regression line is equivalent to the fractal dimension.

3. Results

Pond 2 in the Pielach region of Lower Austria exhibits a variety of vegetation patches with different vertical extents. Therefore, the number of echo pulses recorded in the data set varies between single echo pulses on the land side terrain and multiple echo pulses within the submerged vegetation. This builds an ideal basis for the analysis of the LiDAR waveform structure, as differences in the overall waveform shape can now be analyzed using the tools of the fractal dimension analysis. The results produced by this analysis show a linear dependency between the fractal dimension and the number of detected echo pulses. Furthermore, we compare our human annotation of the waveform data with the results of the calculated fractal dimension.

3.1 Full-waveform shape and fractal dimension values

The application of the box-counting dimension to the recorded waveforms enables us to evaluate the overall waveform characteristic through a single numerical value. The evaluation of the data (Figure 4 and 5) shows that an increase in the fractal dimension indicates a change in the amount of fluctuation within the waveform. In Figure 5, we can observe that a low-return number of echo pulses in the waveform has a fractal dimension close to 0.4, while a high-return number of echo pulses exhibits a fractal dimension of 0.9 for the examples displayed. This, in combination with the larger number of echo

pulses displayed in Figure 4, suggests the hypothesis that an increase in the number of echo pulses recorded is reflected in an increase in the fractal dimension.

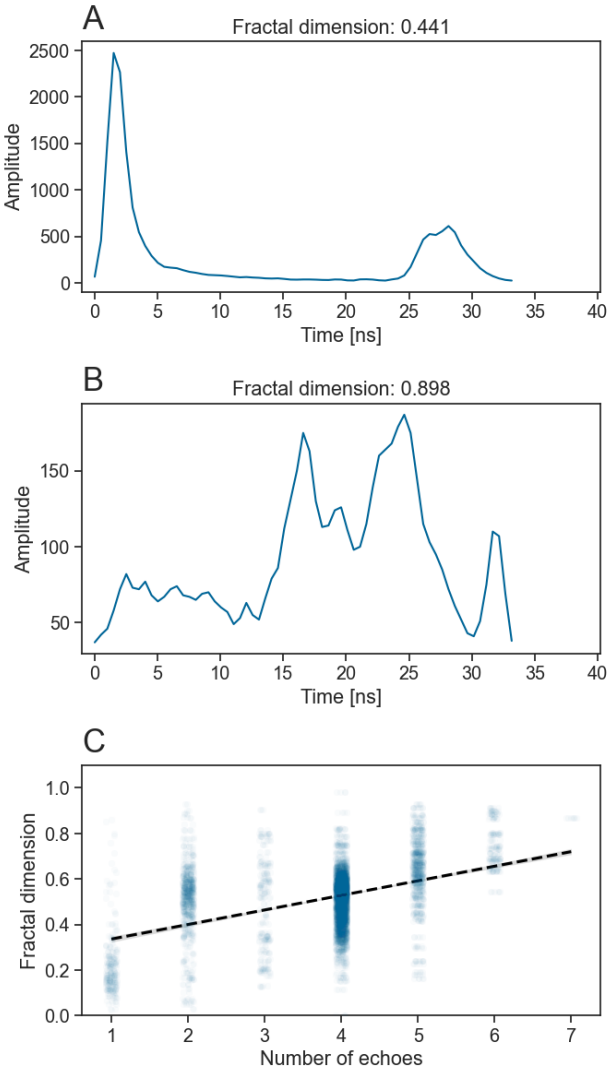

Figure 5. (A) Waveform with two recorded peaks. (B) Waveform with four recorded peaks. (C) Robust regression plot of the fractal dimension in relation to the recorded number of echo pulses by the LiDAR system.

This applies to the cross section shown in Figure 2, as can be seen in Figure 5 C. There, the regression line for the detected numbers of echos displays an increase with increasing fractal dimension. This becomes more apparent by calculating the mean fractal dimension for each number of echos recorded in the analyzed waveform. The corresponding results are shown in Table 2. Except for two waveforms, Table 2 confirms the increase in the fractal dimension with an increasing number of echo pulses. Furthermore, the Pearson correlation and the Spearman correlation for the displayed values are 0.37 and 0.40, respectively, exhibiting a correlation between the fractal dimension and the number of recorded echos. A visual comparison of the measured effect can additionally be seen in Figure 4. There, the fractal dimension and the number of echo pulses (Figure 4 A and B) are high within the same region (the vegetated area of the submerged cross section), while the terrain above the water surface has a low fractal dimension and only single echo pulse waveforms. This can also be seen by separating a subset of waveforms according to the fractal dimension (Figure 4 C and D). To do so, we rounded the fractal dimension to the closest first decimal and plotted the recordings, adjusted to have the same start time. Figure 4 C and D display the described waveforms for fractal dimensions close to 0.8 and 0.3. There, the insight of the fractal dimension into the waveform characteristics becomes apparent, as the waveforms with 0.8 fractal dimension show a large fluctuation in intensity and a large variation in the number of echo pulses, while the waveforms with 0.3 fractal dimension usually contain two distinct returns.

Number echo pulses	1	2	3	4	5	6	7
Frac. dim.	0.22	0.51	0.47	0.5	0.64	0.75	0.87

Table 2. Mean fractal dimension for each number of detected peaks in the waveform, displayed in Figure 5 C.

In summary, the fractal dimensions calculated for the recorded waveforms of the submerged landscape display different numerical values compared to the waveforms of targets on dry land. Therefore, a difference between high and low fractal dimension values is also reflected in the number of returns and the fluctuation within the signal. This introduces a new metric for the analysis of full-waveform LiDAR.

3.2 Comparison to manually annotated data

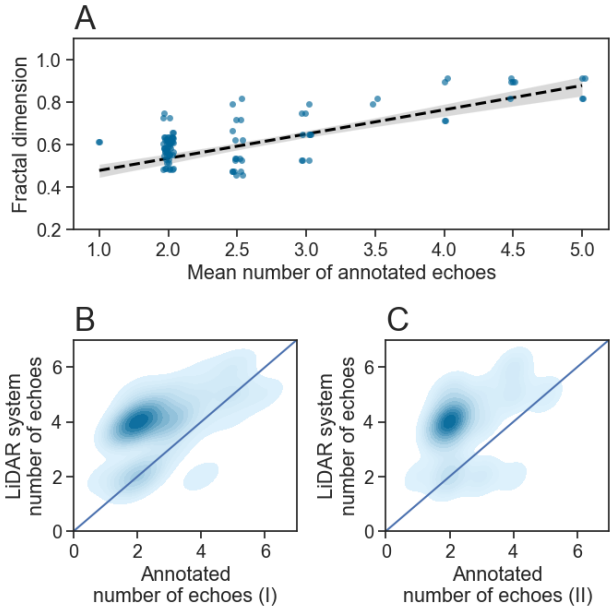

Figure 6. (A) Regression plot of the fractal dimension over the mean number of echo pulses annotated by the two experts. (B-C) Distribution plot of the number of echo pulses extracted during the processing versus the manually annotated peaks.

In order to expand the results, we can compare the fractal dimension to manually annotated labels (Section 2.2) and perform a cross-comparison to the number of echo pulses detected during standard point cloud extraction. The results of this comparison can be seen in Figure 6. There, the first plot displays the mean number of annotated echo pulses, showing a regression trend similar to the results seen in Section 3.1. The main

difference compared to the manual annotation of the subsets can be seen in panels B and C, where for both manually annotated sets of labels, the number of echo pulses produced during the point cloud generation is higher.

Nr. echo pulses	1	2	3	4	5	6
Frac. dim. (AI)	0.61	0.58	0.61	0.79	0.86	0.91
Frac. dim. (AII)	0.61	0.6	0.55	0.87	0.82	-

Table 3. Mean fractal dimension for each echo pulse annotated by the two experts (AI and AII) shown in Figure 6 B and C.

This difference in peak detection can also be seen in the averaged fractal dimension for the annotated peaks (Table 3). There, the first three echo pulses show a much more similar range of values compared to the mean fractal dimension per number of echos shown in Table 2, with an overall higher mean fractal dimension for the annotated echo pulses. These differences in the relation between the fractal dimension and the number of echo pulses also influence the correlation. For annotated echo pulses, the Pearson correlation and Spearman correlation are 0.72 and 0.44, exhibiting an increase in correlation. This highlights a more distinct relationship between both waveform characteristics.

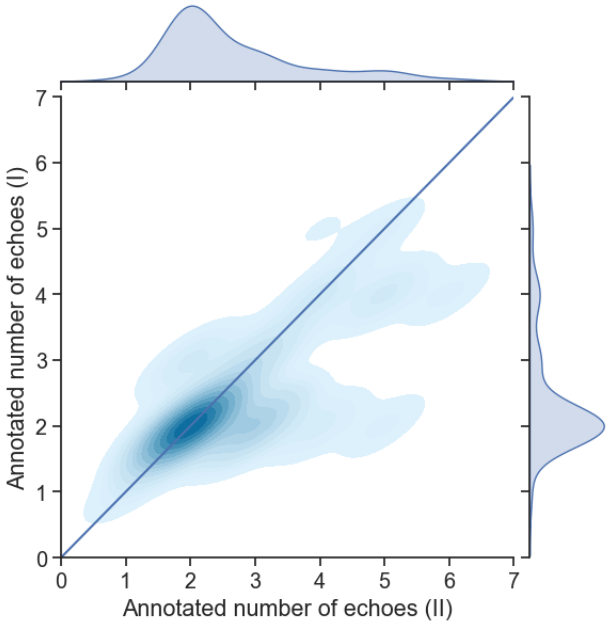

Figure 7. Distribution plot comparing the two manually annotated full-waveform peaks

4. Discussion

The results of Section 3 show a positive correlation between the fractal dimension and the detected peaks of the full-waveform. Furthermore, the standard processing workflow exhibits an overestimation relative to our manually annotated data. To discuss and explain these results, this section explores the underlying challenges in the full-waveform analysis of bathymetric LiDAR.

4.1 Variance in supervised peak detection

The correlation between the fractal dimension and the number of echo pulses displays a similar trend for both manually annotated peaks and extracted echo pulses during standard processing. The main difference for both extraction methods is the number of peaks detected within each waveform. The higher number of echo pulses during standard processing indicates an offset between human annotation and automated detection. In contrast, the labels for both manual annotations match to a large extent, which can be seen in Figure 7. The overestimation of automatic peak detection can be explained by backscattering within the water column and the change of the medium at the water surface, which is a general topic of interest in bathymetric LiDAR (Li et al., 2024; Schwarz et al., 2017). There, the distinction between real and artificial targets (echo pulses) poses a challenge, where multiple methods have been proposed to improve this (Chauve et al., 2009; Li et al., 2024; Schwarz et al., 2019; Xu et al., 2015). Therefore, the insight gained by differentiating the high versus low number of echo pulses based on the fractal dimension offers an alternative parameter to evaluate the waveform independently.

4.2 Fractal dimension as a quality parameter

The increased correlation between the manually annotated peaks and the fractal dimension suggests that the fractal dimension is indicative of what a human would consider a reflected echo. Therefore, the fractal dimension introduced can be used as a quality measure within the waveform processing of full-waveform LiDAR. The results displayed in Section 3 would suggest that a simple filter on two or fewer peaks and more than two peaks in the waveform could be established by using the fractal dimension. Therefore, we fine-tune the echo pulse extraction in the data processing and thus improve agreement between the human impressions of the waveform and the automatically detected echo pulses. However, more research is required to properly evaluate this. In addition, different fields that use LiDAR-based remote sensing, such as forestry, could potentially benefit from the introduced method. In these areas of research, larger challenges remain, as the stronger bottom return causes less distinct self-similarity in the LiDAR waveforms compared to the bathymetric dataset introduced in this study. Therefore, this study only builds a foundation for the general use of the fractal dimension for full-waveform LiDAR.

5. Conclusion

The introduction of the fractal dimension as a measure of the characteristics of the waveform has shown a variety of different results for the analysis of full-waveform LiDAR recordings. The detected positive correlation between the fractal dimension and the number of echo pulses is of particular interest, as this independent measure adds valuable insights for the analysis of laser waveforms. In addition, it allows for an overall separation of different types of waveforms. Furthermore, it should be noted that these correlations can be used to deduct a quality measure of how well the extracted pulses overlap with supervised extractions, which is currently outside the scope of this study. Lastly, the fractal dimension correlates more strongly with the manually annotated labels than with the labels extracted by standard processing methods. This stipulates that an increase in the fractal dimension reflects an increase in real echo pulse count within the waveform. Therefore, the addition of the fractal dimension before classical peak detection could prove advantageous and thus improve the automated echo pulse detection.

This contribution has been peer-reviewed. The double-blind peer-review was conducted on the basis of the full paper.
https://doi.org/10.5194/isprs-annals-X-G-2025-721-2025 | © Author(s) 2025. CC BY 4.0 License.

References

Ai, T., Zhang, R., Zhou, H., Pei, J., 2014. Box-counting methods to directly estimate the fractal dimension of a rock surface. *Applied Surface Science*, 314, 610–621.

BEV, B. f. E.-u. V., 2024. Austrian map online. https://www.bev.gv.at/Services/Produkte/Austrian-Map/Austrian-Map-online.html.

Chauve, A., Vega, C., Durrieu, S., Bretar, F., Allouis, T., Pierrot Deseilligny, M., Puech, W., 2009. Advanced full-waveform lidar data echo detection: Assessing quality of derived terrain and tree height models in an alpine coniferous forest. *International Journal of Remote Sensing*, 30(19), 5211–5228.

Esteller, R., Vachtsevanos, G., Echauz, J., Litt, B., 2001. A comparison of waveform fractal dimension algorithms. *IEEE Transactions on Circuits and Systems I: Fundamental Theory and Applications*, 48(2), 177–183.

Falconer, K., 2014. *Fractal geometry: mathematical foundations and applications*. John Wiley & Sons.

Farmer, J. D., Ott, E., Yorke, J. A., 1983. The dimension of chaotic attractors. *Physica D: Nonlinear Phenomena*, 7(1-3), 153–180.

Fernández-Martínez, M., Sánchez-Granero, M., 2014. Fractal dimension for fractal structures. *Topology and its Applications*, 163, 93–111.

Heinzel, J., Koch, B., 2011. Exploring full-waveform LiDAR parameters for tree species classification. *International Journal of Applied Earth Observation and Geoinformation*, 13(1), 152–160.

Hoyer, J., Saba, M., Dondorp, D., Kolar, K., Esposito, R., Chatzigeorgiou, M., 2020. Mapping calcium dynamics in a developing tubular structure.

Hunter, J. D., 2007. Matplotlib: A 2D graphics environment. *Computing in Science & Engineering*, 9(3), 90–95.

Li, N., Truong, M.-L., Schwarz, R., Pfennigbauer, M., Ullrich, A., 2024. Deep learning assisted exponential waveform decomposition for bathymetric LiDAR. *The International Archives of the Photogrammetry, Remote Sensing and Spatial Information Sciences*, XLVIII-2-2024, 195–202. https://isprs-archives.copernicus.org/articles/XLVIII-2-2024/195/2024/.

Lorenz, E. N., 1963. Deterministic Nonperiodic Flow. *Journal of the Atmospheric Sciences*, 20(2), 130–141.

Mainieri, R., 1993. On the equality of Hausdorff and box counting dimensions. *Chaos: An Interdisciplinary Journal of Nonlinear Science*, 3(2), 119–125.

Mallet, C., Bretar, F., 2009. Full-waveform topographic lidar: State-of-the-art. *ISPRS Journal of Photogrammetry and Remote Sensing*, 64(1), 1–16.

Mallet, C., Soergel, U., Bretar, F., 2008. Analysis of full-waveform lidar data for classification of urban areas. *ISPRS Congress 2008*.

Mandelbrot, B., 1967. How long is the coast of Britain? Statistical self-similarity and fractional dimension. *science*, 156(3775), 636–638.

Mandlburger, G., 2022. A review of active and passive optical methods in hydrography. *The International Hydrographic Review*, 8–52.

Mandlburger, G., Kölle, M., Pöppl, F., Cramer, M., 2023a. Evaluation of Consumer-Grade and Survey-Grade UAV-LIDAR. *The International Archives of the Photogrammetry, Remote Sensing and Spatial Information Sciences*, 48, 99–106.

Mandlburger, G., Pfennigbauer, M., Schwarz, R., Pöppl, F., 2023b. A decade of progress in topo-bathymetric laser scanning exemplified by the pielach river dataset. *ISPRS Annals of the Photogrammetry, Remote Sensing and Spatial Information Sciences*, 10, 1123–1130.

McGuinness, M. J., 1983. The fractal dimension of the Lorenz attractor. *Physics Letters A*, 99(1), 5–9.

Moriguchi, K., 2023. Estimation of fractal dimension of trees using LiDAR point data with sequential data decimation. *Remote Sensing of Environment*, 295, 113722.

Pfeifer, N., Briese, C., 2007. Laser scanning–principles and applications. *Geosiberia 2007-international exhibition and scientific congress*, European Association of Geoscientists & Engineers, cp–59.

Pfennigbauer, M., Ullrich, A., Schwarz, R., 2020. Waveform-averaging airborne laser bathymetry scanner. M. D. Turner, G. W. Kamerman (eds), *Laser Radar Technology and Applications XXV*, SPIE, 19.

Raghavendra, B., Narayana Dutt, D., 2009. A note on fractal dimensions of biomedical waveforms. *Computers in Biology and Medicine*, 39(11), 1006–1012.

RIEGL, 2023. Datasheet riegl vq-840-g.

RIEGL, Laser Measurement Systems GmbH, 2012. LAS Extrabytes Implementation in RIEGL Software WHITEPAPER. *WHITEPAPER*, 12.

Schwarz, R., Mandlburger, G., Pfennigbauer, M., Pfeifer, N., 2019. Design and evaluation of a full-wave surface and bottom-detection algorithm for LiDAR bathymetry of very shallow waters. *ISPRS Journal of Photogrammetry and Remote Sensing*, 150, 1–10.

Schwarz, R., Pfeifer, N., Pfennigbauer, M., Ullrich, A., 2017. Exponential Decomposition with Implicit Deconvolution of Lidar Backscatter from the Water Column. *PFG – Journal of Photogrammetry, Remote Sensing and Geoinformation Science*, 85(3), 159–167.

Sierpinski, W., 1915. Sur une courbe dont tout point est un point de ramification. *CR Acad. Sci.*, 160, 302–305.

Ullrich, A., Pfennigbauer, M., 2011. Echo digitization and waveform analysis in airborne and terrestrial laser scanning. *Photogrammetric week*, 11, 217–228.

Wagner, N., Franke, G., Schmieder, K., Mandlburger, G., 2024. Automatic Classification of Submerged Macrophytes at Lake Constance Using Laser Bathymetry Point Clouds. *Remote Sensing*, 16(13), 2257.

Wagner, W., Ullrich, A., Ducic, V., Melzer, T., Studnicka, N., 2006. Gaussian decomposition and calibration of a novel small-footprint full-waveform digitising airborne laser scanner. *ISPRS Journal of Photogrammetry and Remote Sensing*, 60(2), 100–112.

Wahab, H., 2024. IMPLEMENTING ITERATED FUNCTION-SYSTEMS IN PYTHON. *https://www.math.uni-rostock.de/*.

Xu, L., Li, D., Li, X., 2015. A high success rate full-waveform lidar echo decomposition method. *Measurement Science and Technology*, 27(1), 015205.

Yang, H., Chen, W., Qian, T., Shen, D., Wang, J., 2015. The Extraction of Vegetation Points from LiDAR Using 3D Fractal Dimension Analyses. *Remote Sensing*, 7(8), 10815–10831.